Neural Network Based Parameter Identification for LLC Resonant Converters

Nicholas Green
College of Nanotechnology, Science, and Engineering
University at Albany
Albany, New York, USA
nagreen@albany.edu

Mohammed Agamy
College of Nanotechnology, Science, and Engineering
University at Albany
Albany, New York, USA
magamy@albany.edu

IECON 2024 - 50th Annual Conference of the IEEE Industrial Electronics Society | 978-1-6654-6454-3/24/$31.00 ©2024 IEEE | DOI: 10.1109/IECON55916.2024.10905696

***Abstract*—This paper introduces a neural network based approach for parameter identification of a half-bridge LLC Resonant Converter. By using a set of measured inputs, the system can characterize the component values, and difficult to measure switch characteristics including the junction temperature or gate-source capacitance. This capability is useful for reliability, health monitoring and model based control applications. The range of the Mean Absolute Error (MAE) obtained for all parameters predictions was from 0.142% to 4.12%, with an average MAE of 1.57% over all parameters.**

***Index Terms*—Parameter identification, Digital twin, Neural network, Resonant converters.**

I. Introduction

The concept of a Digital Twin (DT) devises a digital mirror of a physical system. Ideally, the system can update in real-time, with high resolution and accuracy while only having inputs equal to the physical system. When applied to power converters, a DT reveals internal information of the parameters and operation, while minimizing the need for sensor hardware. Achieving this ideal DT is difficult and requires complex models that take into account all the dynamics and physics over the converter's lifetime. Instead, some measurements of the physical system can be taken and fed into a parameter identification block. This block would characterize the converter's state as it changes, update simpler models, and then make predictions. Having this system is perhaps most useful in reliability prediction and lifetime estimation given how difficult those processes are to model.

A variety of techniques have been used to create DTs ranging from statistical modeling, to Machine Learning, or real-time swarm optimization. DT models based on statistical modeling techniques include a Bayesian Optimization approach used in [1] for parameter identification of the resistance, inductance, capacitance, parasitic resistances, and MOSFET on-state resistance of buck and boost converters in an online application. By characterizing the circuit in real-time, the drift of components can be estimated which could be applied for control or repair of converters. In [2], Polynomial Chaos Expansion is used to transform state-space models into stochastic models. Components are assumed to be random variables defined by their tolerances. By modeling the converter and controller, basic condition monitoring can be done by flagging a deviation between the DT and real behavior.

An alternative series of solutions include meta-heuristic optimization algorithms. These algorithms are used to search large solution spaces but have no guarantees of convergence. A population-based technique called Particle Swarm Optimization (PSO) is used by [3]–[7]. PSO works by having a population of guess solutions that work together to search a solution space defined by an objective function. An individual in this swarm balances between its own best solution, the group's best solution, and its current velocity in the search space. Generally these papers try to characterize component values of the converter for health monitoring or control. PSO can constantly search for solutions as the real converter data is gathered and compare them to the DT outputs. In contrast to PSO, one paper uses a technique called Arithmetic Optimization Algorithm (AOA) [8]. AOA makes use of simple arithmetic operations (Addition, Subtraction, Multiplication, and Division) to search over a space. It was shown in [8] that AOA was faster compared to PSO for a Buck Converter model.

Finally, a number of papers have implemented Machine Learning approaches, namely Neural Network variants. An Artificial Neural Network (ANN) is used in [9], [10]. The former paper inputs four PI parameters into the ANN to predict the error between reference and actual active and reactive power. This can be used to tune the control parameters to reduce control error. The latter paper uses an ANN to tune a DT model for accurate predictions. The method of Bayesian Regularized ANN (BR-ANN) and Random Forest (RF) machine learning techniques were applied in [11]. The BR-ANN was trained to predict transient behavior such as settling time, overshoot, rise time, and steady state value. The RF was used to predict steady state ripple through a series of decision trees. To add a dynamic view to the ANN model, methods such as Nonlinear AutoRegressive eXogenous (NARX-ANN) in [12] or a NARX with a Recurrent Neural Network (NARX-RNN) in [13] are used. These models take in inputs over a window of time to predict the converter's outputs building a sense of time into the model itself.

Overall, both statistical and meta-heuristic approaches are computationally demanding and often involve manual modeling, which would have a high level of complexity for incorporating non-linear switch parameters or modeling large

topologies. The machine learning approaches do not experiment with parameter identification at all, and introduce expanded ANN models which may not be necessary. Therefore, this paper introduces an application of machine learning in power electronic converter parameter identification, with a focus on identification of switch parameters using basic ANNs. A case study of an LLC resonant converter operating with variable frequency control is presented to verify the proposed approach.

II. Converter Design

Solid State Transformers (SST) perform the task of regular transformers but can have advantages in size, weight, and power density [14]. Because of the solid state design, more can be done than with just a traditional transformer such as voltage or current regulation for compensation, or fault current limitation [14]. At the core of any SST is an isolated DC-DC converter. LLC resonant converters for SST improves efficiency due to soft switching and adds more control flexibility [15]. This circuit provides a number of opportunities for interesting predictions useful for monitoring involving the switches and resonant tank. Using a detailed switch model enables experimentation with complex predictions about the switch beyond just On-State resistance including the switch capacitances and junction temperatures. Switch information can be useful for health monitoring and control to extend the lifetime of a converter. This will be an important concern for SSTs if they see wide adoption as replacements for conventional transformers.

Modeling the converter will follow the methods in [16] leading to the simplified circuit in Fig. 1. This technique mutates the transformer, rectifier and load resistor into a single AC equivalent resistor at the output of the LLC tank. The gain of the resonant tank can be finally expressed as (1).

$$G = \frac{1}{\left(1 - \left(\frac{\omega_0}{\omega_s}\right)^2 + \frac{L_s}{L_p}\right) + jQ\left(\left(\frac{\omega_0}{\omega_s}\right)^2 \frac{L_s}{L_p} - 1\right)} \quad (1)$$

where, ω_0 is the resonant frequency, ω_s is the switching frequency, Q is the quality factor, L_s and L_p are series and parallel resonant tank inductors, respectively. Here, $Q = \omega_0 C/R_{eq}$ and $\omega_s = \frac{1}{\sqrt{CL_p}}$

A 1200V SiC Cascode JFET model is used [17] to gather detailed switch data. This switch is rated 110A RMS for junction temperatures around 120°C. For simplicity, the converter gain is chosen to be one along with the LLC resonant tank gain. Due to the half-bridge design, a total converter gain of one is achieved using a turns ratio of 1/2. The converter parameters are designed to meet gain requirements as determined by (1). Table I shows the complete converter specifications and component values.

III. Data Collection

The converter simulation is parameterized following the ranges in Table II. Everything else is kept constant including

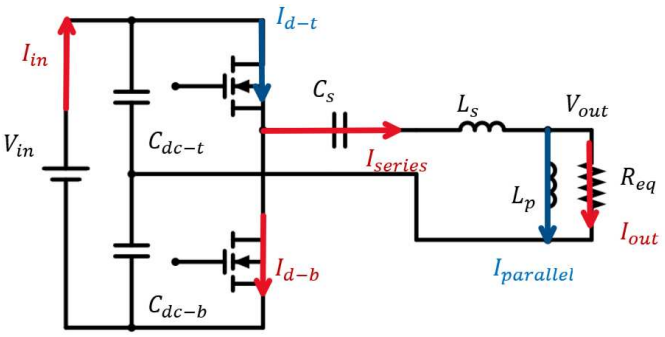

Fig. 1: Simplified Converter with Equivalent Resistor

TABLE I: Converter Specifications

Parameter	Value	Unit
Voltage	800	V
Max Drain Current	110	A RMS
Converter Gain	1	V/V
Resonant Tank Gain	1	V/V
Power	39	kW
Frequency	100	kHz
C_s	239	nF
L_s	10.58	μH
L_p	105.8	μH
R_{eq}	3.325	Ω

the DC-Coupling capacitors, gate voltage, gate resistors, dead-time and switch junction temperature. The loop inductors referenced in the ranges table are located on the top and bottom paths from DC-link capacitors to the switching leg.

The main circuit simulation is coupled with a switch thermal model to estimate temperature rise due to losses. The switch thermal model is represented by a 4R4C thermal circuit as shown in Fig. 2. Switch power is injected as a current source (left) and the case temperature a voltage source (right). Using these, the network will reach a steady state where the final junction temperature can be measured as the leftmost capacitor voltage. The average switch losses are taken from the power circuit simulations. A junction temperature of 140°C was chosen as an average of all scenarios for a conservative estimate of device losses.

Simulations are run one at a time to avoid crashes or stalls. To begin, a random configuration point is chosen from the configuration space defined in Table II. These ranges are subdivided by 32. Using the configuration point, the operating frequency and initial conditions are found. One cycle is given for the rough initial conditions to reach the true steady state, then three cycles are run for the measurements. The power circuit simulation is run, the output of which is used as

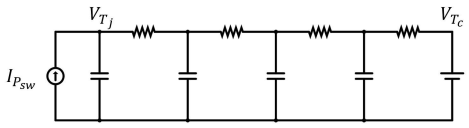

Fig. 2: RC Network Thermal Model

TABLE II: Simulation Parameter Ranges

Parameter	Base Value	Range
C_s	239 nF	$\pm 50\%$
L_s	10.58 μH	$\pm 50\%$
L_p	105.8 μH	$\pm 50\%$
V_{in}	800 V	$\pm 25\%$
C_s ESR	20 mΩ	$\pm 25\%$
C_{DC} ESR	10 mΩ	$\pm 20\%$
Parameter	**Min**	**Max**
Power	1 kW	39 kW
L_{loop}	0.5 nH	20 nH
L_s ESR	10 mΩ	75 mΩ
L_p ESR	10 mΩ	75 mΩ
R_{ds-on}	0 mΩ	50 mΩ
C_{ds}	0 pF	350 pF
C_{gs}	0 pF	8550 pF
T_c	-25 °C	200 °C

input to two thermal simulations. Measurements are taken automatically though LTSpice and are limited to max, min, RMS, or average values over the three cycles. Post-processing can be done for custom measurements. In this case, slew rates were taken with a discrete derivative over a larger window to avoid massive spikes. This is repeated for as many simulations as required.

IV. ANN Modeling

The type of machine learning architecture chosen was a series of Fully Connected ANN's, one each for every desired output. Each network has a series of layers that take in an input vector, pass it through the hidden layers, and finally compute the output. The input and output layer sizes must equal the size of the input and output vectors. The hidden layers were all set to the same size, though the length and size of the hidden layers was tuned manually. The output of each neuron also has a non-linear activation function. Most of these networks will use the Leaky-ReLU with the exception of Zero-Voltage Switching (ZVS) using ReLU. To quantify the success of a network during training the Mean Squared Error (MSE) cost function is used. The Gradient Descent algorithm will adjust the network's weights based on their sensitivity to the loss function. Other hyperparameters include the learning rate, and number of epochs (full training iterations through the whole training set). The full dataset is split in a 70/30 ratio between train and test.

V. Verification

A. Verification Scores

After a network has been trained, the test set is used to see how well the network performs on data it hasn't yet seen. Testing for regression accuracy uses scores that rely on the prediction error such as RMS Error (RMSE) (2), or Mean Absolute Error (MAE) (3). Another score used is the Coefficient of determination or R-Squared (4). This score informs of how well the predictions fit the real outputs by measuring the variance in the predicted data compared to the true data.

$$\text{RMSE} = \sqrt{\frac{1}{N}\sum_{i=1}^{N}(y_i - \hat{y}_i)^2} \tag{2}$$

$$\text{MAE} = \frac{1}{N}\sum_{i=1}^{N}|y_i - \hat{y}_i| \tag{3}$$

$$R^2 = 1 - \frac{\sum_{i=1}^{N}(y_i - \hat{y}_i)^2}{\sum_{i=1}^{N}(y_i - \bar{y})^2} \tag{4}$$

Scoring is done differently for classification tasks. The simplest score is Accuracy which is the ratio of correct predictions to all predictions. Other scores include Precision which is a score defined by the ratio of true positives to all predicted positives (true and false positives). Another score used is named Recall which is the ratio of true positives to all actual positives (true positives and false negatives). In this context, Precision will score how well the identifier can avoid false predictions of ZVS occurring when it has really been lost. Recall scores the identifier's ability to avoid predicting the loss of ZVS when it is still present. Precision may be a more important score because missing the loss of ZVS would increase the switch temperatures and exaggerate degradation. Depending on the application, either Precision or Recall could be more useful. For now, they help benchmark the identifier agnostic of specific application scenarios.

B. Results

This sections presents the best results after training the networks. For the following results a dataset of 108,750 random points was used. The dataset is split in a 70/30 ratio for training and testing. Every regression network used the MSE loss function, while every classification network used the Binary-Cross Entropy loss function, and both have a learning rate of 0.01 using the Adam optimizer. For a complete list of results for each parameter see Table III. Moreover, the input variables are defined in Table IV.

To visualize the results all the predictions were plotted as a scatter plot where the horizontal axis holds the ground truth values, and the vertical axis holds the predicted values. Because the plots' points overlap, it is hard to tell the distribution of predictions. This can be done using a series of box plots. Note that the configuration ranges were subdivided by 32, forming buckets. For each bucket the min, max, first quartile, third quartile, and the median of the predictions were found. These correspond to quantities a box plot uses. To better visualize a series of box plots, the whiskers and box widths are drawn as areas. The larger gray area represents whiskers as a range from the min to max. The smaller blue area represents the box width as the first to third interquartile range. Furthermore, the median of each bucket was plotted as a point. Ideally, the areas would both be very small. Moreover, if the predictions match the ground truths exactly, the median points should lie on a diagonal line represented in red for the figures below. Using this, a complete picture of the results can be created.

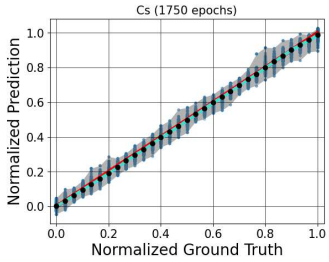

(a) C_s Prediction vs True outputs

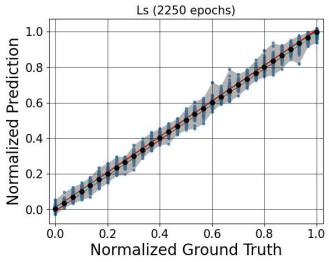

(b) L_s Prediction vs True outputs

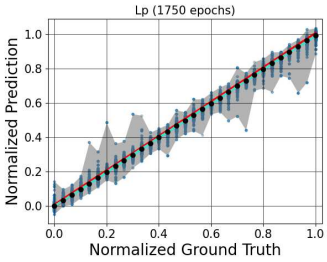

(c) L_p Prediction vs True outputs

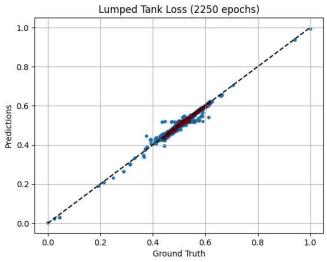

(d) P_{tank} Prediction vs True outputs

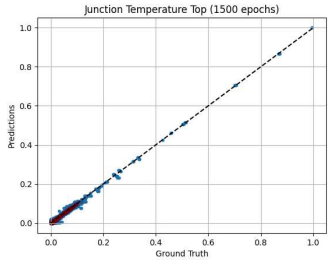

(e) Top T_J Final Prediction vs True outputs

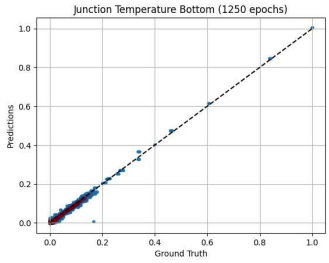

(f) Bottom T_J Final Prediction vs True outputs

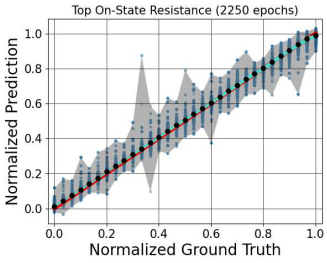

(g) Top R_{ds-on} Final Prediction vs True outputs

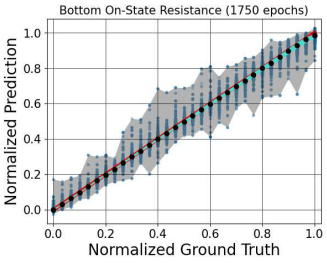

(h) Bottom R_{ds-on} Final Prediction vs True outputs

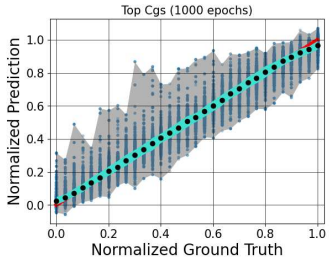

(i) Top C_{gs} Final Prediction vs True outputs

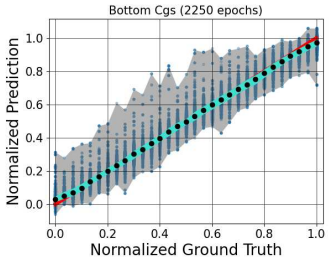

(j) Bottom C_{gs} Final Prediction vs True outputs

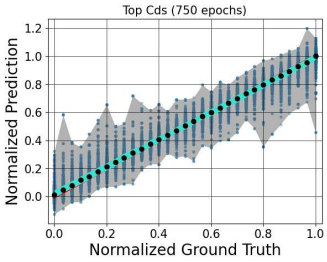

(k) Top C_{ds} Final Prediction vs True outputs

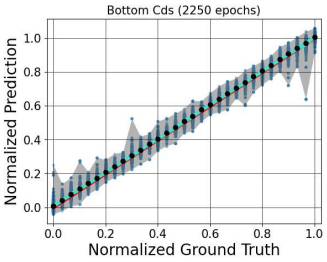

(l) Bottom C_{ds} Final Prediction vs True outputs

Fig. 3: Model predictions vs. ground truth for circuit and operation parameters

TABLE III: Experiment Results

Parameter	RMSE	MAE	R^2
C_s	1.876%	1.411%	99.60%
L_s	1.465%	0.9982%	99.76%
L_p	1.982%	1.284%	99.56%
P_{tank}	0.3489%	0.1420%	97.58%
T_j Top	0.2364%	0.1423%	99.10%
T_j Bottom	0.3103%	0.1912%	98.57%
R_{ds-on} Top	2.480%	1.569%	99.31%
R_{ds-on} Bottom	2.618%	1.530%	99.21%
C_{gs} Top	6.011%	4.115%	95.93%
C_{gs} Bottom	4.891%	3.285%	97.27%
C_{ds} Top	5.684%	3.719%	96.40%
C_{ds} Bottom	2.395%	1.736%	99.35%
Phase Difference	0.4347%	0.2852%	98.73%
Parameter	**Accuracy**	**Precision**	**Recall**
ZVS Top	99.85%	99.98%	99.86%
ZVS Bottom	99.94%	99.98%	99.97%

TABLE IV: Complete Input Measurement Set

Parameter	Description
f_{sw}	Switching Frequency
I_{ser}	LLC Tank Series/Input Current
I_d	Switch Drain Current
V_{gs}	Switch Gate-Source Voltage
V_{ds}	Switch Drain-Source Voltage
V_{ds-on}	Switch Drain-Source Voltage during on-time
V_{rg}	Switch Gate Resistor Voltage
T_c	Switch Case Temperature
Q_g	Gate Charge (Integration of gate current $\frac{V_{rg}}{R_{gate}}$)
$V_{ds-slew}$	Time Derivative of $V_{ds} -> \frac{d}{dt}V_{ds}$
$V_{gs-slew}$	Time Derivative of $V_{gs} -> \frac{d}{dt}V_{gs}$

All switch parameters have corresponding top and bottom measurements for the half-bridge. Also, no single network uses all these inputs

1) Resonant Passives Components: The resonant components did well with low MAEs around 1.2% matched by the high R-Squared of around 99.6%. This can be seen visually in Fig. 3a, 3b, and 3c. Notice the gray area is quite small, and the blue area very small. This means that even the worst

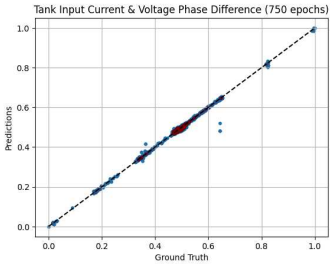

Fig. 4: Resonant Tank Input I-V Phase Difference

predictions were tightly distributed near the ground truth. These networks benefited the most from a widening of the hidden layers to 120 neurons while going further didn't help. Moreover, they had hidden layer lengths of four and did not gain anything from going deeper. The inputs for all the passives included the Max and RMS of I_{series}, I_{out}, I_{in}, and V_{out}. Also included is the DC input voltage, V_{in}, and the switching frequency f_{sw}. The measurements are simple and avoid measuring the high magnitude, high frequency voltages on the passive components. Moreover, the inductors will likely be inaccessible being implicitly designed into the transformer.

2) Lumped Tank Loss: The lumped tank loss performed well with a 0.14% MAE and 97.6% R-Squared. Looking at the scatter plot in Fig. 3d, the predictions generally fall into a central grouping. Looking further into the raw data, it was found that the tank losses are highly biased around a central value. The converter is limited by its normal behavior such that a uniform distribution of tank loses will not be produced within the sweep ranges. This may be a problem for interpolation but looking at the scatter plot again, the rare points outside the dominating grouping still fit quite well. The network structure consisted of four hidden layers with a width of 12. Inputs included the V_{ds-on} of the top and bottom and the maximums of I_{series}, I_{out}, I_{in}, V_{out}, as well as V_{in} and f_{sw}. These inputs should help find the total converter loss, as well as the switch losses, to isolate the tank losses.

3) Junction Temperature: Both the junctions temperatures did well with MAEs at or below 0.19% and an R-Squared near 99%. The scatter plots are presented in Fig.3e and 3f. Similar to the tank loss, these both have the majority of points around a grouping, though still fit the rare points well. Again, the converter dynamics are limited to producing this bias. These networks also had four hidden layers with a width of 12. The inputs important here are similar to the tank losses, in that they need to help isolate the switch losses from total converter losses. These include V_{ds-on} and the maximums of I_{series}, I_{out}, I_{in}, V_{out}, as well as V_{in} and f_{sw}.

4) On-State Resistance: The On-State resistances also did well with MAEs just above 1.5% and an R-Squared around 99.2%. Both of these networks found an optimal hidden layer size of 40 perceptrons and a length of four. Inputs included switch information such as V_{ds-on} min and max, I_d min, max, and RMS, and finally f_{sw}. The top and bottom versions of switch inputs are used respectively. The results are in the scatter plots of Fig. 3g and 3h. While the largest errors can spread wider than before, the majority of the data in the blue follows the line accurately resulting in an accurate prediction.

5) Gate-Source Capacitance: The Gate-Source capacitance can be difficult to estimate properly, though given information about the gate the MAEs can be lowered to around 4% with an R-Squared just above 96%. These networks kept the length of four and performed better as they got wider up to 120 or 90 neurons for the top and bottom. The inputs included the V_{gs} max slew rate, the max and RMS gate charge Q_{gate}, the max and RMS voltage across the external gate resistor V_{rg}, max V_{gs}, and the min V_{ds-on}. The most difficult measurement here would be the slew rate, but this proved important for increasing accuracy. Results are in Fig. 3i and 3j which show a wide worst case error. The interquartile range represented by the blue area shows the network still performs well.

6) Drain-Source Capacitance: The best drain source capacitance networks resulted in MAEs around 3.7% and 1.7% for the top and bottom with an R-Squared 96% and 99% respectively. The scatter plots in Fig. 3k and 3l show good interquartile ranges in blue. The worst errors in gray did well for the bottom but were wider for the top. These networks found an optimal hidden layer width of 120 neurons with a length of four. The min, max, average, and RMS V_{ds} slew rates were included in the inputs along with max Q_{gate}, max V_{gs}, max V_{ds-on}, RMS I_{series}, and f_{sw}. The slew rates proved useful again but are more difficult to measure.

7) Tank Input Voltage and Current Phase Difference: Another parameter is the phase difference between the tank input voltage and input current waveforms. This performed well with an MAE of 0.285% and an R-Squared of 98.7%. The scatter plot is in Fig. 4. This also has a main grouping of samples but the system is still able to accurately predict the rarer points. This network found an optimal hidden layer size of 120 neurons going four deep. The inputs here were the same as the passive component inputs as they relate to the tanks behavior.

8) Zero Voltage Switching: Predicting Zero Voltage Switching suffered from the same problem as the tank loss and junction temperatures. Due to the frequency control used in simulation, ZVS was rarely lost. In the whole dataset, ZVS was true 98.9%, and 99.4% of the time for the top and bottom respectively. One concern is that a network may simply output a constant "true" and never learn to differentiate the negative cases. If this does occur, the Recall score should be 100% from never guessing a negative. Furthermore, the accuracy and precision scores will be the exact same. If these conditions are met, the network is guessing a constant positive and has not learned anything useful. The best results have networks having small widths of 8 and 18 neurons for the top and bottom, both having a length of four. Going deeper or wider did not lead to better results. The final accuracies for the top and bottom were 99.85% and 99.94%, with both precision's at 99.98%. The recall was 99.86% and 99.97% for the top and bottom. The recall was never 100% and the accuracy and precision were never the same showing that the network did

learn to differentiate negative cases. The inputs used include the min, max, average, and RMS V_{ds} slew rates, max I_{series}, max Q_{gate}, and f_{sw}. These should help predict the speed C_{ds} can be discharged and therefore if ZVS will occur.

C. Discussion

The proposed ANN model shows good prediction performance over the design space of the converter. The model depends on inputs that are standard to measure in the power or gate drive circuit. Even though a few of the parameters have tight distributions, such as lumped tank losses, junction temperature, phase difference and ZVS indication, the model is considered sufficient since the regression output is limited to interpolation of results. Even with a skewed dataset the network can do a good job of discriminating rare outputs that deviate from the main peak. Looking at the scatter plots for the tank loss, both junctions temperatures, and the phase difference (Fig. 3d, 3e, 4, and 3f) do show a good fit suggesting the network can successfully follow points outside the main peak when rare. Errors in the results could be attributed to the dataset quality or size. Quality meaning numerical error from simulation or pre-processing stages, as well as the breadth of modes a converter is simulated through. Network tuning could also play a role as some output variables may require deeper networks for longer chains of calculations.

VI. Conclusion

This paper applied simple Feed Forward Neural Networks to an LLC Resonant converter to create a parameter identifier. It is shown to be capable of predicting internal component values including the switch parameters. By following a procedure of parameterizing a converter, many simulations can be run by randomly sampling from chosen ranges of those parameters. Using the collected data, simple neural networks can be trained to predict each output. Results here show MAEs below 4.12% for all parameters. As many of the measurements required as inputs are simple values taken over multiple cycles, the system could feasibly be used for parameter identification. The developed models are computationally simple being straight forward ANNs, making them well suited for implementation on local converter FPGAs. This approach can be readily applied to non-resonant converters. Further, adding a detailed transformer model would enable the extension of this approach to isolated converters.

References

[1] S. Chen, S. Wang, P. Wen, and S. Zhao, "Digital Twin for Degradation Parameters Identification of DC-DC Converters Based on Bayesian Optimization," in *2021 IEEE International Conference on Prognostics and Health Management (ICPHM)*. Detroit (Romulus), MI, USA: IEEE, Jun. 2021, pp. 1–9.

[2] M. Milton, C. De La O, H. L. Ginn, and A. Benigni, "Controller-Embeddable Probabilistic Real-Time Digital Twins for Power Electronic Converter Diagnostics," *IEEE Transactions on Power Electronics*, vol. 35, no. 9, pp. 9850–9864, Sep. 2020. [Online]. Available: https://ieeexplore.ieee.org/document/8984243/

[3] G. Di Nezio, M. Di Benedetto, A. Lidozzi, and L. Solero, "Digital Twin based Real-Time Analysis of DC-DC Boost Converters," in *2022 IEEE Energy Conversion Congress and Exposition (ECCE)*. Detroit, MI, USA: IEEE, Oct. 2022, pp. 1–7. [Online]. Available: https://ieeexplore.ieee.org/document/9947394/

[4] M. T. Fard and J. He, "Digital Twin Health Monitoring of Five-Level ANPC Power Converter based on Estimation of Semiconductor On-State Resistance," in *2023 IEEE Industry Applications Society Annual Meeting (IAS)*. Nashville, TN, USA: IEEE, Oct. 2023, pp. 1–7. [Online]. Available: https://ieeexplore.ieee.org/document/10406700/

[5] Y. Gong, Y. Tian, C. Wen, H. Luo, C. Li, and W. Li, "Digital Twin Based Condition Monitoring for High Power Converters," in *2022 IEEE International Power Electronics and Application Conference and Exposition (PEAC)*. Guangzhou,Guangdong, China: IEEE, Nov. 2022, pp. 892–897. [Online]. Available: https://ieeexplore.ieee.org/document/9959161/

[6] Y. Peng, S. Zhao, and H. Wang, "A Digital Twin Based Estimation Method for Health Indicators of DC–DC Converters," *IEEE Transactions on Power Electronics*, vol. 36, no. 2, pp. 2105–2118, Feb. 2021. [Online]. Available: https://ieeexplore.ieee.org/document/9141430/

[7] Q. Wu, W. Wang, Q. Wang, L. Xiao, and B. Hu, "Digital Twin Approach for Degradation Parameters Identification of a Single-Phase DC-AC Inverter," in *2022 IEEE Applied Power Electronics Conference and Exposition (APEC)*. Houston, TX, USA: IEEE, Mar. 2022, pp. 1725–1730. [Online]. Available: https://ieeexplore.ieee.org/document/9773462/

[8] S. Rajendran, V. S. K. Devi, and M. Diaz, "Digital twin based identification of degradation parameters of DC-DC converters using an Arithmetic Optimization Algorithm," in *2022 3rd International Conference for Emerging Technology (INCET)*. Belgaum, India: IEEE, May 2022, pp. 1–5. [Online]. Available: https://ieeexplore.ieee.org/document/9824058/

[9] X. Cheng, J. Chen, Y. Chen, X. Zhao, Z. Zhou, Q. Yang, and N. Y. Dai, "Digital-Twin-Driven PI Parameter Evaluation Method for Grid-Connected Converters," in *2023 4th International Conference on Power Engineering (ICPE)*. Macau, Macao: IEEE, Dec. 2023, pp. 26–31. [Online]. Available: https://ieeexplore.ieee.org/document/10469163/

[10] X. Song, T. Jiang, S. Schlegel, and D. Westermann, "Parameter tuning for dynamic digital twins in inverter-dominated distribution grid," *IET Renewable Power Generation*, vol. 14, no. 5, pp. 811–821, Apr. 2020. [Online]. Available: https://onlinelibrary.wiley.com/doi/10.1049/iet-rpg.2019.0163

[11] H. S. Krishnamoorthy and T. Narayanan Aayer, "Machine Learning based Modeling of Power Electronic Converters," in *2019 IEEE Energy Conversion Congress and Exposition (ECCE)*. Baltimore, MD, USA: IEEE, Sep. 2019, pp. 666–672. [Online]. Available: https://ieeexplore.ieee.org/document/8912608/

[12] A. Wunderlich and E. Santi, "Digital Twin Models of Power Electronic Converters Using Dynamic Neural Networks," in *2021 IEEE Applied Power Electronics Conference and Exposition (APEC)*. Phoenix, AZ, USA: IEEE, Jun. 2021, pp. 2369–2376. [Online]. Available: https://ieeexplore.ieee.org/document/9487201/

[13] G. Rojas-Duenas, J.-R. Riba, K. Kahalerras, M. Moreno-Eguilaz, A. Kadechkar, and A. Gomez-Pau, "Black-Box Modelling of a DC-DC Buck Converter Based on a Recurrent Neural Network," in *2020 IEEE International Conference on Industrial Technology (ICIT)*. Buenos Aires, Argentina: IEEE, Feb. 2020, pp. 456–461. [Online]. Available: https://ieeexplore.ieee.org/document/9067098/

[14] Xu She and A. Huang, "Solid state transformer in the future smart electrical system," in *2013 IEEE Power & Energy Society General Meeting*. Vancouver, BC: IEEE, 2013, pp. 1–5. [Online]. Available: http://ieeexplore.ieee.org/document/6672768/

[15] D. Dong, M. Agamy, J. Bebic, Q. Chen, and G. Mandrusiak, "A modular sic high-frequency solid-state transformer for medium-voltage applications: Design, implementation, and testing," *IEEE Journal of Emerging and Selected Topics in Power Electronics*, vol. 7, no. 2, pp. 768–778, Jun. 2019.

[16] R. Steigerwald, "A comparison of half-bridge resonant converter topologies," *IEEE Transactions on Power Electronics*, vol. 3, no. 2, pp. 174–182, Apr. 1988. [Online]. Available: https://ieeexplore.ieee.org/document/4347/

[17] "1200V-8.6mW SiC FET," Qorvo, UF3SC120009K4S Datasheet, Dec. 2019.